ENVIRONMENTAL RESEARCH
COMMUNICATIONS

INCLUSIVE PUBLISHING TRUSTED SCIENCE

Part of the ENVIRONMENTAL RESEARCH SERIES

PURPOSE-LED PUBLISHING™

LETTER • OPEN ACCESS

A comparison of radar and optical remote sensing to detect cyclone-induced canopy disturbance in two subtropical forest landscapes

To cite this article: Jonathan Peereman *et al* 2022 *Environ. Res. Commun.* **4** 101002

Environmental Research Communications

LETTER

A comparison of radar and optical remote sensing to detect cyclone-induced canopy disturbance in two subtropical forest landscapes

Jonathan Peereman[1], **Soyeon Bae**[2] and **Teng-Chiu Lin**[1,*]

[1] Department of Life Science, National Taiwan Normal University, No 88 section 4, Ting-Chow Road, Taipei 11677, Taiwan
[2] Technische Universität München, Hans-Carl-von-Carlowitz-Platz 2, 85354 Freising Munchen, Bayern 80333, Germany
* Author to whom any correspondence should be addressed.

E-mail: tclin@ntnu.edu.tw

Keywords: disturbance ecology, cyclone, subtropical forest, vegetation indices, radar, optical

Supplementary material for this article is available online

OPEN ACCESS

RECEIVED
11 August 2022

REVISED
12 September 2022

ACCEPTED FOR PUBLICATION
29 September 2022

PUBLISHED
10 October 2022

Abstract

Optical remote sensing is a tool frequently used to assess cyclone-induced forest disturbances. However, the frequent cloud cover limits the availability of optical data in cyclone basins. On the other hand, radar remote sensing is not affected by cloud cover and has been used to detect windthrows. Yet, the potential of radar sensing in monitoring cyclone damages of varying magnitudes across forest landscapes remains unclear. Here, we compared radar remote sensing to optical remote sensing of four cyclone disturbances in the Fushan Experimental Forest of northern Taiwan and the El Yunque National Forest in Puerto Rico using Landsat 8 and C-band Sentinel-1 satellite data. We analyzed the change in two optical vegetation indices, EVI (Enhanced Vegetation Index) and NDII (Normalized Difference Infrared Index), and three radar-based metrics, co- and cross-polarized backscatters (VV, VH) and their ratio (Canopy Development Index, CDI) after cyclone disturbances and during approximately the same periods of non-cyclone years. We assessed the improved temporal resolution permitted by Sentinel-1 constellation on the detection of forest canopy disturbance. Bootstrapped comparisons indicated that both optical and radar indices detected canopy change, but their correlations were not significant. Improved temporal resolution of CDI allowed to distinguish cyclone-induced canopy change from the phenological variation and even change by nearby cyclones. Although this, VV and VH backscatters responded more closely to cyclone disturbances than their ratio. Our results demonstrate that the C-band backscatter intensities can track cyclone-induced change of forest canopies, and provide an assessment of C-band capabilities to monitor cyclone disturbances.

1. Introduction

Tropical cyclones are major disturbances of forest landscapes, with rain- and wind-mediated damages ranging from light defoliation, branch fall, to tree death through wind throw or broken boles [1]. As a result, cyclones influence carbon sequestration [2], and their effect on carbon stocks may be exacerbated by the observed shift of their trajectories toward coasts and higher latitudes [3, 4], and change in frequency and intensity [5, 6].

The effects of cyclone disturbance on forest landscapes have been widely assessed using passive optical remote sensing techniques, such as vegetation indices (VIs), that relies on canopy reflectance within the blue to shortwave infrared spectrum [7–10]. However, optical remote sensing is limited by clouds which can be present in a significant portion of scenes either seasonally or thorough the year, especially in humid regions [11, 12]. High cloudiness therefore limits the study of forest dynamics and disturbances that relies on multidate imagery and common pixels across images [8, 10]. As shown in figure 1 for the subtropical Fushan Experimental Forest

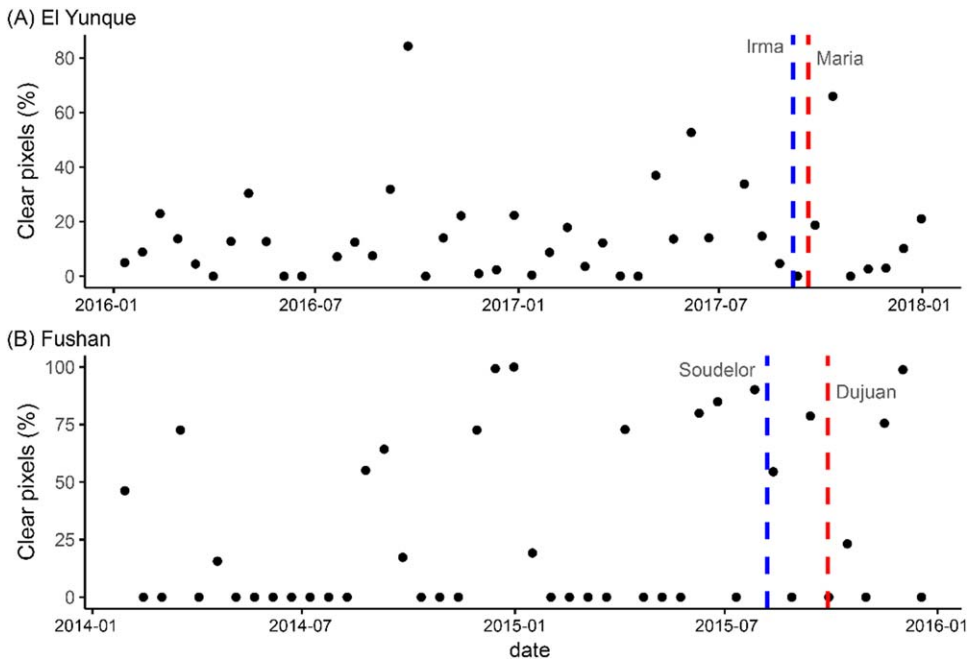

Figure 1. Proportions of cloud free pixels in the El Yunque National Forest in Puerto Rico (A, total pixels = 129283), and the Fushan Experimental Forest in northern Taiwan (B, total pixels = 12104) in Level-2 Collection-2 Landsat 8 images over two consecutive years (one without and one with cyclones ⩾ category 3). Cyclone occurrences are indicated with dashed lines. The list of scenes is shown in Supporting Information table S1.

(FEF) of Taiwan and the El Yunque National Forest (EYNF) in Puerto Rico, clouds and cloud shadows can represent high proportions of pixels in tropical mountain forests, making diachronic studies difficult.

Forest landscapes have also been studied with synthetic aperture radar-based imagery (SAR) [7, 13]. Unlike optical remote sensing, radar is not affected by clouds and illumination. Moreover, whereas optical remote sensing is mostly responding to biochemical properties of the surfaces, radar backscatter responds to surface physical structure and its dielectric constant that is related to moisture [14, 15] and temperature [16]. Radar can be emitted in different wavelengths, from X- and C-bands (2.4–7.5 cm) to P- and L-bands (15–100 cm). X- and C-bands mostly interact with smaller elements of the forest, such as leaves and smaller branches [14, 17], and thus are stopped within the canopy whereas longer wavelengths penetrate deeper and interact with larger elements such as trunks and primary branches [17–19]. In addition, SAR studies used the horizontal and vertical polarizations of transmitted signals that interact differently with the variable orientations of forest components [20], such as branches [14, 15].

As a result, radar remote sensing has been used to study forest dynamics [21–24] and characteristics [25–27], and to follow the effects of different disturbances on forested landscapes [7]. Bae *et al* [28] demonstrated that C-band can accurately monitor insect-mediated defoliation and recovery of a mixed-oak forest canopy. Cyclone disturbances have been also studied using SAR, with several studies focusing on floods as both short and long wavelengths can produce accurate identification based on the strong water-related change in radar backscatter [29]. Additionally, a few studies have analyzed cyclone-induced stand destruction and identified windthrows using co- and cross-polarizations [30–32].

The Sentinel-1 constellation [33] provides C-band SAR data dating back to 2014 (launch of Sentinel-1A). The use of Sentinel-1 data over annual scales permitted to show that co- and cross-polarized backscatter at those wavelengths respond to canopy phenology or disturbance [23, 24, 28, 34], reaching results that can be comparable or better than those produced using optical remote sensing [35, 36]. Sentinel-1 imagery has a finer temporal resolution (6-days at the equator) than L-band based imagery (revisit interval of a few weeks) which allows monitoring canopy damage quickly after disturbance with good accuracy [34, 37]. This is particularly important for assessing cyclone damage and recovery in the subtropical region because most cyclones occur in the warm growing season during which substantial phenological change could occur with a few weeks. Moreover, Sentinel-1 imagery is freely available unlike L-band imagery. There has been extensive forest disturbances monitoring based on Sentinel-1, covering vectors such as caterpillars [28], fires [35, 38], and logging [39]. Moreover, it has been successfully used for automated detection of forest loss in the tropics [40, 41]. However, in relation with cyclone disturbances, Sentinel-1 data has mainly been used to detect floods [29, 42, 43] or effects on temperate forest canopies[32, 34]. Thus, it is unclear whether Sentinel-1 C-band is able to detect

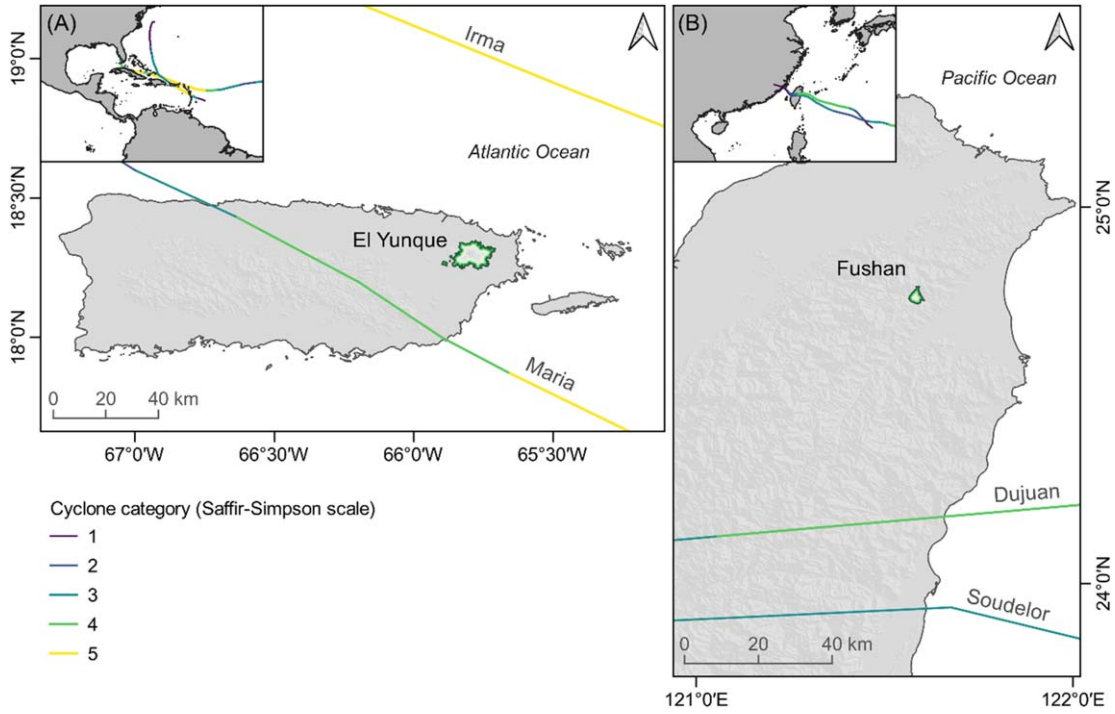

Figure 2. Locations of the El Yunque National Forest in Puerto Rico (A) and the Fushan Experimental Forest in northern Taiwan (B) and studied cyclone paths according to the International Best Track Archive for Climate Stewardship [45, 46].

cyclone-induced change across tropical and subtropical forests where damages are generally not as severe as large blowdowns.

Assessment of the potential of freely available C-band satellites to monitor cyclone-induced canopy disturbances would provide valuable information on the alternative they represent to optical sensors that are generally limited by clouds in tropical forests and regions affected by cyclones [8, 11]. Here we compared the forest canopy change measured with Sentinel-1 backscatter to the change of widely used VIs derived from Landsat 8 data after the passage of cyclones in Puerto Rico and Taiwan. Both islands experience frequent major cyclones, with five hurricanes and 37 typhoons $\geqslant$ category 3 on the Saffir-Simpson scale [44] passing within 100km of Puerto Rico and Taiwan, respectively, between 1980 and 2021 according to the International Best Track Archive for Climate Stewardship archive (IBTrACS) [45, 46]. We assessed whether the cyclone-induced change in the intensity of co- and cross-polarized backscatters and their ratio fit the variation detected by optically sensed VIs over the same period. Then, we computed the instantaneous change in backscatter between the closest scenes before and after disturbance and compared it to backscatter change measured along with the optical data, which often spread over a wider time interval, in order to study the effect of the delay caused by cloudiness. Because the severity of cyclone induced tree damage is much higher in Puerto Rico than in Taiwan [47], this study also assessed whether Sentinel-1 monitoring also applies to locations with very different cyclone damage severities.

2. Materials and methods

2.1. Site and cyclone selection

Site and cyclone selection was based on the availability of non-cloudy multispectral images and Sentinel-1 data, and on the occurrence of major cyclones. The EYNF (11336 ha; altitude 150–1065 meters) is located on the Luquillo Mountains in eastern Puerto Rico (figure 2). Hurricanes Irma (2017/09/06) and María (2017/09/20) passed at 23 and 69 km from EYNF. The FEF (1097 ha, 400–1400 meters) is a natural reserve of northern Taiwan (figure 2). Typhoon Soudelor (2015/08/07, category 3) and Typhoon Dujuan (2015/09/28, category 4) crossed Central Taiwan at 92 and 65 km from FEF. Noticeable damages and increased litterfall have been reported in the two forests following these four cyclones [48–51].

2.2. Data

Studied sites were delimited using shapefiles from the World Database on Protected Areas for the EYNF [52], and from Dr Chung-Te Chang for FEF. The cyclone tracks and strengths on the Saffir-Simpson scale were identified in the IBTrACS archives.

For each disturbance event, Landsat 8 scenes within two months before and after the cyclone passage were downloaded from the USGS Earthexplorer portal (earthexplorer.usgs.gov) as Collection 2 Level-2 products of 30-meters spatial resolution. Collection 2 Level-2 scenes are the product of the LaSRC and CFmask algorithms [53, 54] which create surface reflectance bands and a pixel quality assessment band identifying areas not obstructed by clouds or shadows. In addition, we selected scenes recorded during the similar period in the following years to monitor changes associated with plant phenology. Because of cloud cover over the EYNF (figure 1), Landsat 8 data did not permit to study Irma and María individually, hence the two hurricanes were studied together using Landsat 8 but independently using Sentinel-1. On the other hand, Soudelor and Dujuan could be studied separately with both Landsat 8 and Sentinel-1, using one scene to describe pre- or post-disturbance. Sentinel-2 data was not used because there is no available Sentinel-2 scene to assess forest canopy state before Soudelor and Dujuan.

For the comparison of Landsat 8 optical and Sentinel-1 SAR data, we selected Sentinel-1 scenes within 7-days before and after the Landsat 8 scene collection in order to minimize phenological variation. However, we increased the range to 10-days for the image preceding Soudelor because no data was available within 7-days. Only scenes from the ascending orbit and from the same paths (62 for EYNF, 69 for FEF) were used because different relative orbits show slight variation (see figure S1). Then, to assess whether SAR data recorded immediately before and after disturbance could provide an advantage in disturbance detection, we selected the closest Sentinel-1 data before and after each disturbance event. Sentinel-1 data were downloaded from the Copernicus Open Access Hub of the ESA (scihub.copernicus.eu/dhus) as ground range detected (GRD) products of 10-meters spatial resolution acquired using the interferometric wide-swath mode (IW). The products had two bands corresponding to the co-polarized vertical radar transmission and reception (VV), and to cross-polarized vertical radar transmission and horizontal reception (VH). All Landsat 8 and Sentinel-1 scenes are listed in Supporting Information table S1.

2.3. Processing

2.3.1. Pre-processing

Topographical correction was applied to all Landsat 8 bands using 30-m ASTER-global DEM and the 'topCor' function of the *RStoolbox* package in R 4.0.3 [55–57].

Sentinel-1 data was pre-processed using the method described by Bae *et al* [58] that relies on the Sentinel-1 Toolbox within the Sentinel Application Platform software. After precise orbit correction, the thermal and border noises were removed. The data was then radiometrically calibrated into the radar brightness coefficient (beta naught, β°). Using 1-arc-second spatial resolution Shuttle Radar Topography Mission DEM, terrain flattening was applied on the β° to produce the backscatter coefficient γ° (gamma naught), which was then terrain corrected in order to account for local illumination. Finally, the γ° products were aligned with the Landsat 8 products, and resampled to the 30-meters resolution using bilinear interpolation.

2.3.2. Indices to monitor vegetation change

We computed two VIs commonly used to monitor tropical forest dynamics, including their change associated with cyclones [59–61]. The Enhanced Vegetation Index (EVI) [62] is based on blue, red, and near-infrared (NIR) bands, and is computed using coefficients adjusting for aerosol resistance and ground effect. The Normalized Difference Infrared Index (NDII) [63] is calculated using NIR and shortwave infrared. NDII is sensitive to leaf water content, and has been used to monitor change in tropical forest canopies [59, 61, 64, 65].

C-band co- and cross-polarized backscatters are affected differentially by characteristics of forest canopies such as leaf area or AGB [15, 21, 26]. Moreover, co- and cross-polarizations have been shown to have different sensitivities to windthrows [27, 66] and to soil moisture [67]. The ratio between co- and cross-polarized backscatters of C-bands has been used to monitor forest biophysical parameters, including vegetation disturbance [23, 27, 28, 37]. Therefore, we used the Canopy Development Index (CDI, equation (3)) [28], that combines VV and VH backscatters. CDI was computed as the difference between the average over 15 days of the resampled VV and VH backscatters converted to decibels with $10 \times \log_{10}(\gamma^{\circ})$, henceforth referred to as γ°_{VV} and γ°_{VH}.

$$\mathrm{CDI} = \gamma^{0}_{VV} - \gamma^{0}_{VH} \tag{3}$$

The effect of cyclones on forest structure was assessed by computing the differences between pre- and post-cyclone VI values (*i.e.*, pre-disturbance VI—post-disturbance VI), defined as ΔVI here. Similarly, we computed the change of γ°_{VV}, γ°_{VH}, and CDI, referred to as ΔVV, ΔVH, and ΔCDI. Indeed, forest canopy disturbances generally induce a decrease in VIs [10, 60, 68], and they can affect the γ°_{VV} / γ°_{VH} ratio [28] as backscatters change [38].

2.4. Analysis

2.4.1. Optical- and SAR-based canopy change detection

Cyclone-induced change was assessed in two steps. First, we compared pre- and post-cyclone values using bootstrapped comparisons on means as $\text{mean}_{\text{pre-cyclone}}$—$\text{mean}_{\text{post-cyclone}}$ with resampling and 5000 iterations to compute 95% confidence intervals (95% CIs). However, the computed difference did not separate the cyclone effect from phenological effect, thus the change (i.e., Δ) measured during the cyclone year was compared with the change computed over the similar period during non-cyclone years. It used the same bootstrapped approach as $\text{mean change}_{\text{cyclone year}}$—$\text{mean change}_{\text{non-cyclone year}}$.

Correlations between the ΔEVI, ΔNDII, and ΔCDI were analyzed using the 'corr.test' function of the *psych* package [69] adjusting *p* using Holm's method.

2.4.2. Effect of temporal resolution

We investigated the role of temporal resolution on the assessment of cyclone damages by comparing the values of CDI measured approximately at the same time as the Landsat 8 images (defined here as wide interval) to those measured immediately before and after the cyclone disturbances (short interval). We used the method of Herberich *et al* [70] for multiple comparisons using *multcomp* and *sandwich* packages [71, 72] to compare all CDI groups (i.e., CDI before and after cyclone, at short or wide interval). Finally, we computed Spearman's correlation coefficients between ΔCDI measured over the wide and the short intervals.

3. Results

3.1. Optical and SAR detected canopy change

Significant differences were detected between pre- and post-cyclone states in both El Yunque National Forest ($n = 3118$ pixels) and Fushan Experimental Forest ($n = 4235$ pixels) (figure 3, table S2). Canopy damage can be observed following Irma-María, and Dujuan, as EVI and NDII had significantly dropped ($\Delta\text{VI} > 0$ based on bootstrapped comparisons of the means). However, after Typhoon Soudelor, EVI and NDII increased (EVI, 0.57 ± 0.002 to 0.60 ± 0.002; NDII, 0.32 ± 0.001 to 0.33 ± 0.001). Interestingly, during non-cyclone years, most of the VIs also significantly changed, with some change directions identical to those for the cyclone year (table S2). Similar to EVI and NDII, the SAR-based index, CDI, decreased after Hurricanes Irma and María (6.57 ± 0.027 to 5.66 ± 0.021, 95% CI of 0.837;0.975; figure 3(A)). Unlike EVI and NDII, CDI decreased after Soudelor (6.80 ± 0.023 to 6.53 ± 0.024) and did not change after Dujuan (6.60 ± 0.023 to 6.61 ± 0.017). Backscatter consistently increased after the cyclones in EYNF and FEF (figure 3; table S2).

The comparison of ΔVIs, ΔVV, ΔVH, and ΔCDI measured during cyclone- and non-cyclone years at similar time periods indicated that they had different magnitudes of change (table 1). EVI and NDII decreased more sharply after the passage of Irma-María, and Dujuan than during non-cyclone years (95% CIs > 0, table 1). On the other hand, ΔEVI following Soudelor was negative whereas ΔEVI of the similar period in 2017 was positive (95% CI of -0.053;-0.037). NDII increased after Soudelor but less so than over the similar period in 2017 (95% CI of 0.011;0.0158, figure 3, table S2). The decrease of CDI after Irma-María was significantly greater than that over the similar period of the non-cyclone year (95% CI > 0). ΔCDI associated with Soudelor was not significantly different from ΔCDI measured in the similar period of 2017 in the absence of disturbance (0.270 ± 0.032 and 0.203 ± 0.032, 95% CI -0.023;0.156). Similarly, the decrease of CDI associated with Dujuan was not significantly different than that measured in the similar period of 2018 (0.042 ± 0.021, 95% CI -0.121;0.022). ΔVV and ΔVH associated with cyclones were significantly greater than for non-cyclone years (95% CI < 0; table 1) during which $\gamma^{\circ}_{\text{VV}}$ and $\gamma^{\circ}_{\text{VH}}$ did not always significantly change (figure 3, table S2).

ΔEVI and ΔNDII were positively correlated for all cyclones ($0.53 < \rho < 0.76$; $p < 0.001$; table S3). On the other hand, the ΔCDI did not have significant correlations with ΔEVI and ΔNDII.

3.2. Temporal resolution and disturbance monitoring of SAR

In EYNF, the use of SAR scenes closer to Irma and María passage than Landsat 8 imagery permitted to study the individual effect of each disturbance. CDI significantly varied among the five points in the timeline (figure 4(A), tables S4–5). CDI decreased between the first image and the last image (6.71 ± 0.004 to 5.33 ± 0.003), which are the two time points with available optical images, as well as over the two short intervals including the two hurricanes (i.e., from 6.75 ± 0.004 to 5.94 ± 0.004 for Irma, and from 5.94 ± 0.004 to 5.27 ± 0.004 for María). CDI increased significantly between the value measured around the time of the Landsat 8 scene (i.e., the first), and the value measured right before the landfall of the first hurricane, Irma (i.e., the second), and between the value immediately after Hurricane María (i.e., the fourth) and the first Landsat 8 scene available after María (i.e., the fifth).

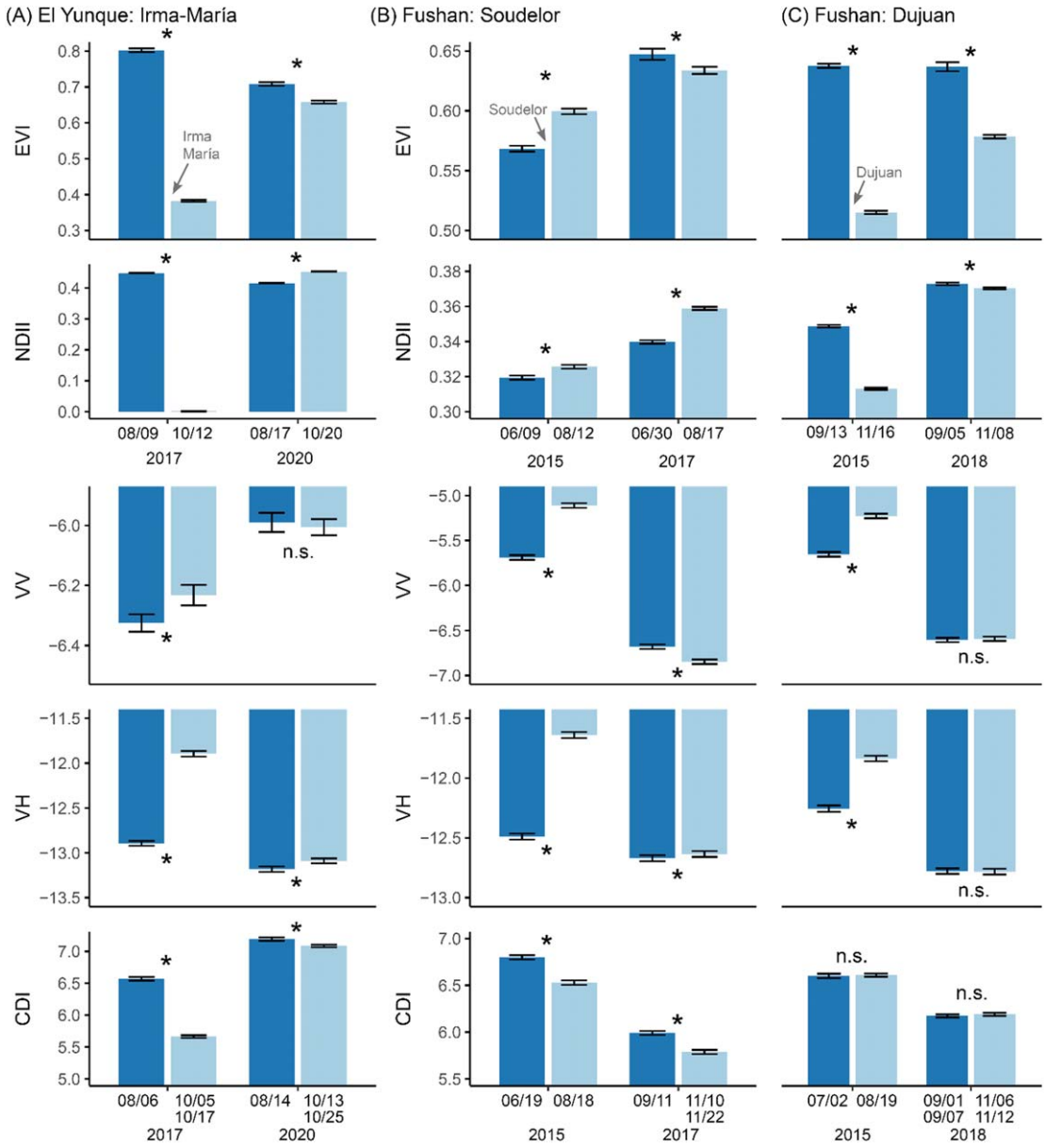

Figure 3. Enhanced Vegetation Index (EVI), Normalized Difference Infrared Index (NDII), VV and VH backscatter (dB), and Canopy Development Index (CDI) before and after cyclone passages in 2017 at the El Yunque National Forest (A, $n = 3118$) of Puerto Rico and in 2015 at the Fushan Experimental Forest (B and C, $n = 4235$) of northern Taiwan for common pixels across scenes (i.e., excluding clouds and their shadows). Bars represent the standard error. Years without cyclones are shown for comparison for each site: 2020 for Irma and María, 2017 for Soudelor, and 2018 for Dujuan. Landsat 8 and Sentinel-1 data acquisition dates are indicated. Significant (*) and non-significant (n.s.) differences between mean pre- and post-cyclone values are indicated based on 95% confidence intervals computed through bootstrapped comparisons on means (table S2).

In FEF, the CDI showed the same decreasing pattern between the wide and close intervals for both Typhoons Soudelor and Dujuan (figure 4(B), table S4). However, CDI increased over a month between the two post-cyclone images after Soudelor (08/18 and 09/11) and after Dujuan (10/05 and the average of 11/10 and 11/22).

Although significant ($p < 0.001$), the correlations were weak between ΔCDI of wide and short intervals ($\rho = 0.07$) measured before and after Irma and María passage in EYNF. In FEF, ΔCDI of wide and short intervals had $\rho = 0.48$ ($p < 0.001$) for Soudelor and $\rho = 0.56$ ($p < 0.001$) for Dujuan.

4. Discussion

Our study showed that both optical-based VIs and the SAR-based backscatters and their ratio responded to cyclone-induced change of subtropical forest canopies, but their responses were not always similar. Most VIs had decreased post disturbance, reflecting the decrease in vegetation cover following cyclone passage as has been reported in other studies of these cyclones [9, 68, 73], but there were exceptions (i.e. the increase of VIs) after

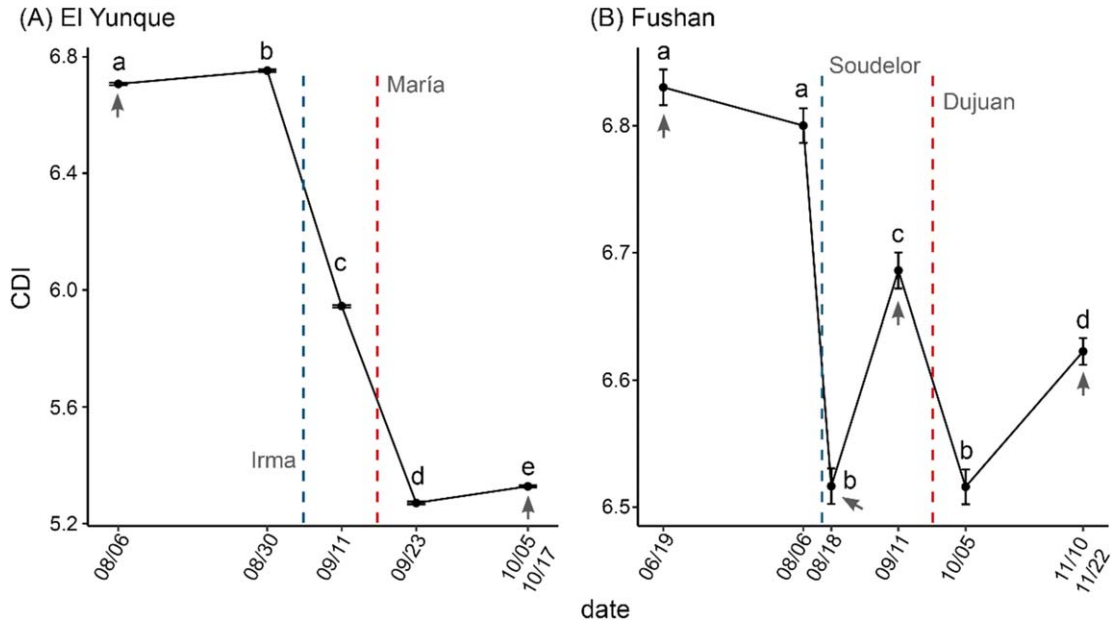

Figure 4. Mean Canopy Development Index (CDI, with standard error) before and after four cyclones (dashed lines) in the El Yunque National Forest of Puerto Rico (A, 2017) and the Fushan Experimental Forest of northern Taiwan (B, 2015) according to Sentinel-1 scenes taken around the time Landsat-8 scenes were recorded (arrows), and at the dates the closest to the cyclone passages. Different letters above points denote significant differences according to the 95% confidence intervals computed between each group (table S5). Note: Post-Soudelor and Pre-Dujuan scenes are used for both short- and wide-intervals because of their proximity to the Landsat-8 scenes acquisition time and to the typhoons passage. Variation in VV and VH backscatters is shown in figures S2-S3.

Table 1. Means and standard errors (SE) of change in Enhanced Vegetation Index (ΔEVI), Normalized Difference Infrared Index (ΔNDII), and Canopy Development Index (ΔCDI) before and after cyclone (year in bold) and for years without cyclone at the same season. The 95% confidence intervals (95% CI) are computed through bootstrapped comparisons on means as the difference between Δ of the cyclone year minus Δ of the non-cyclone year with a sample size *n* and 5000 iterations. All the differences between the paired years were significant except for ΔCDI at Fushan for both Typhoons Soudelor and Dujuan.

	Mean (SE)	Mean (SE)	95% CI of the two-years difference
El Yunque ($n = 3118$)			
Irma & María	2017	2020	
ΔEVI	0.42 (0.004)	0.051 (0.004)	0.357;0.381
ΔNDII	0.45 (0.002)	−0.04 (0.001)	0.480;0.489
ΔVV	−0.09 (0.038)	0.02 (0.024)	−0.197;−0.020
ΔVH	−1.00 (0.035)	−0.09 (0.024)	−0.991;−0.821
ΔCDI	0.91 (0.033)	0.11 (0.033)	0.705;0.890
Fushan ($n = 4235$)			
Soudelor	2015	2017	
ΔEVI	−0.031 (0.001)	0.014 (0.004)	−0.053;−0.037
ΔNDII	−0.006 (0.001)	−0.019 (0.001)	0.011;0.015
ΔVV	−0.58 (0.022)	0.17 (0.022)	−0.809;−0.685
ΔVH	−0.84 (0.022)	−0.04 (0.022)	−0.877;−0.750
ΔCDI	0.270 (0.032)	0.203 (0.032)	−0.023;0.156
Dujuan	2015	2018	
ΔEVI	0.123 (0.002)	0.058 (0.004)	0.056;0.072
ΔNDII	0.036 (0.001)	0.003 (0.001)	0.031;0.035
ΔVV	−0.43 (0.020)	−0.01 (0.016)	−0.464;−0.363
ΔVH	−0.42 (0.021)	0.004 (0.016)	−0.475;−0.370
ΔCDI	−0.008 (0.028)	−0.02 (0.023)	−0.064;0.082

Typhoon Soudelor. CDI and VV and VH backscatters showed more consistent changes than VIs after cyclones. CDI decreased after cyclones (figure 3, table 1) agreeing with the change caused by insect disturbance [28], while VV and VH backscatters increased (figure 3, table 1) in accordance with the change observed after windthrows [32].

The significant effect of cyclones was seen through their comparison to non-cyclone years (figure 3, table 1). The comparison with non-cyclone years is important in assessment of cyclone-induced change when vegetation

experiences phenological changes over the studied period. We detected significant changes in optical and radar-based metrics during years without cyclones that are likely explained by the phenological variation [74], suggesting that the variation in VI and radar backscatter after cyclone passage is the combined product of phenology and disturbance. Hence, after early cyclones, phenological-induced increase of VI and CDI may obscure the cyclone-induced drop in VI and CDI, as shown in the increase of VI after Soudelor, while VI and CDI drop associated with late cyclones could be cofounded with the decrease in photosynthetic activity and canopy cover, respectively, leading to overestimation of cyclone damage severity. Such obstacle in detecting disturbance was intensified by wide intervals of around two months between available cloud-free optical images.

With such wide two-months intervals between SAR images during the vegetation growing season, CDI also cannot avoid failing to distinguish the canopy change caused by cyclones, as shown with the Typhoons Soudelor and Dujuan (figure 4). However, CDI over the short intervals (c.a., 12 days) significantly detected canopy change before and after the two typhoons in Taiwan and even respective changes over the two consecutive Hurricanes Irma and María in two weeks (figure 4) while Landsat did not provide cloud-free images between the two hurricanes. Sentinel-1 VV and VH bands, and their ratio have been used to automate the detection of forest loss over tropical landscapes [40, 41]. Moreover, the CDI has been shown to respond to highly variable dynamics by caterpillar-mediated canopy defoliation and successive refoliation [28]. Our results showed another possible application of Sentinel-1, the rapid return rate of which can allow observing the abrupt change in forest canopy after cyclones, distinguishing it from changes driven by other factors and even by nearby cyclones.

Interestingly, VV and VH backscatter intensities consistently showed distinct increases after cyclones compared to non-cyclone years, even in the wide interval analysis. Substantial increases of both VV and VH intensities by cyclones caused relatively small changes of CDI a ratio index using the different sensitivities of VV and VH polarizations to volume scattering and double bounce [75, 76]. The backscatter change may not only be explained by vegetation damage [20]. Backscatter change is probably related to LAI or overall biomass variation as C-band is mostly interacting with the canopy [18, 26, 77]. However, backscatter also likely responded to variation in surface humidity [78] after cyclone passage that influence SAR backscatter of tropical forest floor and canopy ([79, 80] with L-band). Besides, increased backscatter might be also attributed to the increased entropy [81] stemming from modification of structural complexity and surface roughness by cyclones. Although drivers of backscatter change are not clear, our study showed that VV and VH backscatters intensities are more effective than CDI for detecting cyclone disturbance effects.

We assume that the different disturbance magnitudes and characteristics of cyclones influenced the effectiveness of VIs, SAR backscatters, and CDI in monitoring disturbance effects. Indeed, Puerto Rican forests display greater cyclone-induced damages than Taiwan forests [47], as evident from the greater drop in VIs and CDI and jump in SAR backscatter in EYNF than in FEF. Soudelor and Dujuan were weaker than Irma and María, and EVI and NDII increased after Soudelor and CDI had no change after Dujuan. VI-increase observed after Soudelor is likely due to mild upper canopy damage and the reflectance of remaining understory vegetation. Additionally, we postulate that Soudelor's legacy interacted with the passage of Dujuan. Increased vulnerability in some parts of the forest canopy, such as changes of soil stability and tree weakening [82–85], may explain the sharper drop of VIs following Dujuan. Nevertheless, comparing cyclones is complex as reported by Feng *et al* [9] in the North Atlantic, partly because they have different wind speeds and rainfall [86, 87].

Across the two sites, SAR remote sensing appeared to be advantageous because cloudy pixels Landsat images represented a significant part of the total (88% for Irma-María, 46% for Soudelor, and 33% for Dujuan). The area occulted by clouds would grow if we were to include images of non-cyclone years or analyze canopy recovery. Nevertheless, across cloudy regions, atmospheric moisture may have an effect on the SAR signal. Further research is needed to assess whether the radar-based detection of cyclone-induced fine scale canopy change is affected by frequent cloudiness.

Several studies based on optical and SAR remote sensing have suggested that their combination could improve forest monitoring in comparison with the use of optical or SAR alone, even if SAR-role is marginal [39, 88–90]. For instance, Cornforth *et al* [91] had monitored changes in mangroves, including changes induced by cyclones, using a combination of optical and SAR L-band imagery. Our results confirm these observations for cyclone disturbances and suggest that Sentinel-1 C-band helped understanding landscape dynamics immediately after disturbance. Thus, this study adds another possible use of Sentinel-1 in combination with Landsat imagery for tropical cyclone research besides the recent analysis of cyclone floods [29]. It is likely that VV and VH backscatters, and VIs tracked different changes in the forest landscape, including change other than vegetation disturbance as SAR responds to a wider range of parameters (e.g., temperature, rainfall) [20]. Therefore, their complementary use mitigates the effect of their respective limiting factors such as clouds, underlayer reflectance, and moisture effects [92, 93]. Yet, our interpretation of VV and VH change across the two forest landscapes was limited by the lack of field data. Future ground-based assessments of cyclone disturbances are necessary to understand the relationships between canopy change and the variation in VV and VH backscatters at finer scales.

5. Conclusions

We found that, alike EVI and NDII, γ°_{VV} and γ°_{VH}, and their ratio (CDI) permitted to detect canopy change following cyclones in comparison to pre-disturbance and to non-cyclone years. VV and VH backscatters showed greater disturbance responses than CDI, because the change of CDI was mitigated by the same increases of VV and VH after cyclones. The use of SAR permitted to improve forest landscape representation, as cloudy and cloud-free pixels could be monitored. Additionally, the finer temporal resolution permitted by the cloud-independence of radar sensors indicated rapid canopy responses to cyclone disturbances in both subtropical forests. Our results demonstrated that C-band co-polarized and cross-polarized backscatters can be used to monitor cyclone disturbances. Because the relationship between optical- and radar-based vegetation indices is unclear, further research should resolve the links between site-observed canopy change and the dynamics of γ°_{VV} and γ°_{VH} associated with cyclone disturbance.

Acknowledgments

We thank Dr Chung-Te Chang (Adam) for providing the shapefile of the Fushan reserve. We acknowledge the use of Copernicus Sentinel-1 and Landsat 8 data. This research is supported by the Ministry of Science and Technology (grant numbers 108–2313-B-003–001 -MY3, 110–2811-B-003–502).

Data availability statement

All data that support the findings of this study are included within the article (and any supplementary files).

Conflicts of interest

The authors declare no conflicts of interest.

ORCID iDs

Jonathan Peereman https://orcid.org/0000-0002-5128-3536
Soyeon Bae https://orcid.org/0000-0003-1961-1226
Teng-Chiu Lin https://orcid.org/0000-0003-1088-8771

References

[1] Lugo A E 2008 Visible and invisible effects of hurricanes on forest ecosystems: an international review *Austral Ecol.* **33** 368–98
[2] Chambers J Q, Fisher J I, Zeng H, Chapman E L, Baker D B and Hurtt G C 2007 Hurricane Katrina's Carbon Footprint on U.S. Gulf Coast Forests *Science* **318** 1107-
[3] Altman J *et al* 2018 Poleward migration of the destructive effects of tropical cyclones during the 20th century *Proc. Natl Acad. Sci. USA* **115** 11543–8
[4] Wang S and Toumi R 2021 Recent migration of tropical cyclones toward coasts *Science* **371** 514
[5] Liu K S and Chan J C L 2020 Recent increase in extreme intensity of tropical cyclones making landfall in South China *Clim. Dyn.* **55** 1059–74
[6] Sun Y, Zhong Z, Li T, Yi L, Hu Y, Wan H, Chen H, Liao Q, Ma C and Li Q 2017 Impact of ocean warming on tropical cyclone size and its destructiveness *Sci Rep.* **7** 8154
[7] Frolking S, Palace M W, Clark D B, Chambers J Q, Shugart H H and Hurtt G C 2009 Forest disturbance and recovery: A general review in the context of spaceborne remote sensing of impacts on aboveground biomass and canopy structure *J. Geophys. Res. Biogeosci.* **114** G00E2
[8] de Beurs K M, McThompson N S, Owsley B C and Henebry G M 2019 Hurricane damage detection on four major Caribbean islands *Remote Sens. Environ.* **229** 1–13
[9] Feng Y, Negrón-Juárez R I and Chambers J Q 2021 Multi-cyclone analysis and machine learning model implications of cyclone effects on forests *Int. J. Appl. Earth Obs. Geoinf.* **103** 102528
[10] Peereman J, Hogan J A and Lin T-C 2022 Disturbance frequency, intensity and forest structure modulate cyclone-induced changes in mangrove forest canopy cover *Global Ecol. Biogeogr.* **31** 37–50
[11] Asner G P 2001 Cloud cover in Landsat observations of the Brazilian Amazon *Int. J. Remote Sens.* **22** 3855–62
[12] Hansen M C, Krylov A, Tyukavina A, Potapov P V, Turubanova S, Zutta B, Ifo S, Margono B, Stolle F and Moore R 2016 Humid tropical forest disturbance alerts using Landsat data *Environ. Res. Lett.* **11** 034008
[13] Shugart H H, Saatchi S and Hall F G 2010 Importance of structure and its measurement in quantifying function of forest ecosystems *J. Geophys. Res. Biogeosci.* **115** G00E13
[14] Chuah H T and Tan H S 1992 A radar backscatter model for forest stands *Waves Random Media* **2** 7–28
[15] Westman W E and Paris J F 1987 Detecting forest structure and biomass with C-band multipolarization radar: Physical model and field tests *Remote Sens. Environ.* **22** 249–69

[16] Way J *et al* 1990 The effect of changing environmental conditions on microwave signatures of forest ecosystems: preliminary results of the March 1988 Alaskan aircraft SAR experiment *Int. J. Remote Sens.* **11** 1119–44
[17] Chauhan N S, Lang R H and Ranson K J 1991 Radar modeling of a boreal forest *IEEE Trans. Geosci. Remote Sens.* **29** 627–38
[18] Lucas R M, Moghaddam M and Cronin N 2004 Microwave scattering from mixed-species forests, Queensland, Australia *IEEE Trans. Geosci. Remote Sens.* **42** 2142–59
[19] Proisy C, Mougin E, Fromard F, Trichon V and Karam M A 2002 On the influence of canopy structure on the radar backscattering of mangrove forests *Int. J. Remote Sens.* **23** 4197–210
[20] Kasischke E S, Bourgeau-Chavez L L, Christensen N L and Haney E 1994 Observations on the sensitivity of ERS-1 SAR image intensity to changes in aboveground biomass in young loblolly pine forests *Int. J. Remote Sens.* **15** 3–16
[21] Proisy C, Mougin E, Dufrene E and Dantec V L 2000 Monitoring seasonal changes of a mixed temperate forest using ERS SAR observations *IEEE Trans. Geosci. Remote Sens.* **38** 540–52
[22] Yu Y and Saatchi S 2016 Sensitivity of L-Band SAR Backscatter to Aboveground Biomass of Global Forests *Remote Sens.* **8** 522
[23] Frison P-L, Fruneau B, Kmiha S, Soudani K, Dufrêne E, Le Toan T, Koleck T, Villard L, Mougin E and Rudant J-P 2018 Potential of sentinel-1 data for monitoring temperate mixed forest phenology *Remote Sens.* **10** 2049
[24] Rüetschi M, Schaepman M E and Small D 2018 Using multitemporal sentinel-1 C-band backscatter to monitor phenology and classify deciduous and coniferous forests in Northern Switzerland *Remote Sens.* **10** 55
[25] Cougo M F, Souza-Filho P W M, Silva A Q, Fernandes M E B, Dos Santos J R, Abreu M R S, Nascimento W R Jr and Simard M 2015 Radarsat-2 backscattering for the modeling of biophysical parameters of regenerating mangrove forests *Remote Sens.* **7** 17097–112
[26] Kovacs J M, Vandenberg C V and Flores-Verdugo F 2006 Assessing fine beam RADARSAT-1 backscatter from a white mangrove (Laguncularia racemosa (Gaertner)) canopy *Wetlands Ecol. Manage.* **14** 401–8
[27] Kovacs J M, Jiao X, Flores-de-Santiago F, Zhang C and Flores-Verdugo F 2013 Assessing relationships between Radarsat-2 C-band and structural parameters of a degraded mangrove forest *Int. J. Remote Sens.* **34** 7002–19
[28] Bae S, Müller J, Förster B, Hilmers T, Hochrein S, Jacobs M, Leroy B M L, Pretzsch H, Weisser W W and Mitesser O 2022 Tracking the temporal dynamics of insect defoliation by high-resolution radar satellite data *Methods Ecol.* **13** 121–132
[29] DeVries B, Huang C, Armston J, Huang W, Jones J W and Lang M W 2020 Rapid and robust monitoring of flood events using Sentinel-1 and Landsat data on the Google Earth Engine *Remote Sens. Environ.* **240** 111664
[30] Fransson J E S, Walter F, Blennow K, Gustavsson A and Ulander L M H 2002 Detection of storm-damaged forested areas using airborne CARABAS-II VHF SAR image data *IEEE Trans. Geosci. Remote Sens.* **40** 2170–5
[31] Asbridge E, Lucas R, Rogers K and Accad A 2018 The extent of mangrove change and potential for recovery following severe tropical cyclone yasi, hinchinbrook Island, Queensland, Australia *Ecol Evol.* **8** 10416–34
[32] Rüetschi M, Small D and Waser L T 2019 Rapid detection of windthrows using sentinel-1 C-band SAR DATA *Remote Sens.* **11** 115
[33] Torres R *et al* 2012 GMES Sentinel-1 mission *Remote Sens. Environ.* **120** 9–24
[34] Tomppo E, Ronoud G, Antropov O, Hytönen H and Praks J 2021 Detection of forest windstorm damages with multitemporal SAR data—a case study: Finland *Remote Sens.* **13** 383
[35] Pepe A, Stroppiana D, Calo F, Imperatore P, Boschetti L, Bignami C, Brivio P A and Lanari R 2018 Exploitation of Copernicus Sentinels data for sensing fire-disturbed vegetated areas *IGARSS 2018 – 2018 IEEE Int. Geoscience and Remote Sensing Symp. (Valencia, Spain, 22-27 July 2018)* pp 7589–92
[36] Reiche J *et al* 2021 Forest disturbance alerts for the Congo Basin using Sentinel-1 *Environ. Res. Lett.* **16** 024005
[37] Hoekman D, Kooij B, Quiñones M, Vellekoop S, Carolita I, Budhiman S, Arief R and Roswintiarti O 2020 Wide-area near-real-time monitoring of tropical forest degradation and deforestation using sentinel-1 *Remote Sens.* **12** 3263
[38] Lohberger S, Stängel M, Atwood E C and Siegert F 2018 Spatial evaluation of Indonesia's 2015 fire-affected area and estimated carbon emissions using Sentinel-1 *Global Change Biol.* **24** 644–54
[39] Hirschmugl M, Deutscher J, Sobe C, Bouvet A, Mermoz S and Schardt M 2020 Use of SAR and Optical Time Series for Tropical Forest Disturbance Mapping *Remote Sens.* **12** 727
[40] Bullock E L, Healey S P, Yang Z, Houborg R, Gorelick N, Tang X and Andrianirina C 2022 Timeliness in forest change monitoring: a new assessment framework demonstrated using Sentinel-1 and a continuous change detection algorithm *Remote Sens. Environ.* **276** 113043
[41] Shimizu K, Ota T and Mizoue N 2019 Detecting forest changes using dense landsat 8 and sentinel-1 time series data in tropical seasonal forests *Remote Sens.* **11** 1899
[42] Lin Y N, Yun S-H, Bhardwaj A and Hill E M 2019 Urban flood detection with sentinel-1 multi-temporal synthetic aperture radar (SAR) observations in a bayesian framework: a case study for hurricane matthew *Remote Sens.* **11** 1778
[43] Mondal P, Dutta T, Qadir A and Sharma S 2022 Radar and optical remote sensing for near real-time assessments of cyclone impacts on coastal ecosystems *Remote Sens Ecol Conserv. n/a* **8** 506–20
[44] Simpson R H and Riehl H 1981 *The hurricane and its impact.* (Baton Rouge, LA: Louisiana State University Press) p 398
[45] Knapp K R, Diamond H J, Kossin J P, Kruk M C and Schreck C J 2018 *International best track archive for climate stewardship (IBTrACS) projectVersion 4. [IBTrACS.ALL.list.v04r00]* NOAA National Centers for Environmental Information (https://doi.org/10.25921/82ty-9e16)
[46] Knapp K R, Kruk M C, Levinson D H, Diamond H J and Neumann C J 2010 The International best track archive for climate stewardship (IBTrACS): unifying tropical cyclone best track data *B Am Meteorol Soc.* **91** 363–76
[47] Lin T-C, Hogan J A and Chang C-T 2020 Tropical cyclone ecology: a scale-link perspective *Trends Ecol. Evol.* **7** 594–604
[48] Lin S-Y, Shaner P-J L and Lin T-C 2018 Characteristics of old-growth and secondary forests in relation to age and typhoon disturbance *Ecosystems.* **21** 1521–32
[49] Liu X, Zeng X, Zou X, González G, Wang C and Yang S 2018 Litterfall production prior to and during hurricanes irma and maria in four puerto rican forests *Forests.* **9** 367
[50] Uriarte M, Thompson J and Zimmerman J K 2019 Hurricane maría tripled stem breaks and doubled tree mortality relative to other major storms *Nat. Commun.* **10** 1362
[51] Zimmerman J K, Wood T E, González G, Ramirez A, Silver W L, Uriarte M, Willig M R, Waide R B and Lugo A E 2021 Disturbance and resilience in the luquillo experimental forest *Biol Conserv.* **253** 108891
[52] UNEP-WCMC I 2021 *Protected Planet: The World Database on Protected Areas (WDPA)* (Cambridge, UK: UNEP-WCMC and IUCN) Available from (https://protectedplanet.net/en)
[53] Foga S, Scaramuzza P L, Guo S, Zhu Z, Dilley R D Jr, Beckmann T, Schmidt G L, Dwyer J L, Hughes M J and Laue B 2017 Cloud detection algorithm comparison and validation for operational Landsat data products *Remote Sens. Environ.* **194** 379–90
[54] Vermote E, Justice C, Claverie M and Franch B 2016 Preliminary analysis of the performance of the Landsat 8/OLI land surface reflectance product *Remote Sens. Environ.* **185** 46–56

[55] Core R 2020 *Team. R: A Language and Environment for Statistical Computing.* (Vienna, Austria: R Foundation for Statistical Computing)
[56] Leutner B, Horning N and Schwalb-Willmann J (2022) RStoolbox: Tools for remote sensing data analysis *R package version 0.3.0*
[57] Riano D, Chuvieco E, Salas J and Aguado I 2003 Assessment of different topographic corrections in Landsat-TM data for mapping vegetation types (2003) *IEEE Trans. Geosci. Remote Sens.* **41** 1056–61
[58] Bae S *et al* 2019 Radar vision in the mapping of forest biodiversity from space *Nat. Commun.* **10** 4757
[59] Gang C, Pan S, Tian H, Wang Z, Xu R, Bian Z, Pan N, Yao Y and Shi H 2020 Satellite observations of forest resilience to hurricanes along the northern Gulf of Mexico *For Ecol Manage.* **472** 118243
[60] Rossi E, Rogan J and Schneider L 2013 Mapping forest damage in northern nicaragua after hurricane felix (2007) using MODIS enhanced vegetation index data *GIsci Remote Sens.* **50** 385–99
[61] Zhang K, Thapa B, Ross M and Gann D 2016 Remote sensing of seasonal changes and disturbances in mangrove forest: a case study from South Florida *Ecosphere.* **7** e01366
[62] Huete A R, Didan K, Miura T, Rodriguez E P, Gao X and Ferreira L G 2002 Overview of the radiometric and biophysical performance of the MODIS vegetation indices *Remote Sens. Environ.* **83** 195–213
[63] Hardisky M A, Klemas V and Smart R M 1983 The influence of soil salinity, growth form, and leaf moisture on the spectral reflectance of *Spartina alterniflora* canopies *Photogramm Eng Remote Sensing.* **49** 77–83
[64] Cheng Y-B, Zarco-Tejada P J, Riaño D, Rueda C A and Ustin S L 2006 Estimating vegetation water content with hyperspectral data for different canopy scenarios: relationships between AVIRIS and MODIS indexes *Remote Sens. Environ.* **105** 354–66
[65] Lagomasino D, Fatoyinbo T, Castañeda-Moya E, Cook B D, Montesano P M, Neigh C S R, Corp L A, Ott L E, Chavez S and Morton D C 2021 Storm surge and ponding explain mangrove dieback in southwest florida following hurricane irma *Nat. Commun.* **12** 4003
[66] Green R M 1998 The sensitivity of SAR backscatter to forest windthrow gaps *Int. J. Remote Sens.* **19** 2419–25
[67] Huang X, Ziniti B, Torbick N and Ducey M J 2018 Assessment of forest above ground biomass estimation using multi-temporal c-band sentinel-1 and polarimetric l-band PALSAR-2 data *Remote Sens.* **10** 1424
[68] Hu T and Smith R B 2018 The impact of Hurricane Maria on the vegetation of Dominica and Puerto Rico using multispectral remote sensing *Remote Sens.* **10** 827
[69] Revelle W (2022) Psych: Procedures for Psychological, Psychometric, and Personality Research. *R package version 2.2.3*
[70] Herberich E, Sikorski J and Hothorn T 2010 A robust procedure for comparing multiple means under heteroscedasticity in unbalanced designs *PLoS One* **5** e9788
[71] Hothorn T, Bretz F and Westfall P 2008 Simultaneous inference in general parametric models *Biom J.* **50** 346–63
[72] Zeileis A, Köll S and Graham N 2020 Various versatile variances: an object-oriented implementation of clustered covariances in R *J Stat Softw.* **95** 36
[73] Peereman J, Hogan J A and Lin T-C 2020 Assessing typhoon-induced canopy damage using vegetation indices in the Fushan Experimental Forest, Taiwan *Remote Sens.* **12** 1654
[74] Chang C-T, Wang S-F, Vadeboncoeur M A and Lin T-C 2014 Relating vegetation dynamics to temperature and precipitation at monthly and annual timescales in Taiwan using MODIS vegetation indices *Int. J. Remote Sens.* **35** 598–620
[75] Mitchard E T A *et al* 2012 Mapping tropical forest biomass with radar and spaceborne LiDAR in Lopé National Park, Gabon: overcoming problems of high biomass and persistent cloud *Biogeosciences.* **9** 179–91
[76] Saatchi S 2019 SAR methods for mapping and monitoring forest biomass *The SAR Handbook: Comprehensive Methodologies for Forest Monitoring and Biomass Estimation.* ed A I Flores-Anderson, K E Herndon, R B Thapa and E Cherrington (Huntsville: NASA) pp 207–46
[77] Lucas R M, Cronin N, Lee A, Moghaddam M, Witte C and Tickle P 2006 Empirical relationships between AIRSAR backscatter and LiDAR-derived forest biomass, Queensland, Australia *Remote Sens. Environ.* **100** 407–25
[78] Twele A, Cao W, Plank S and Martinis S 2016 Sentinel-1-based flood mapping: a fully automated processing chain *Int. J. Remote Sens.* **37** 2990–3004
[79] Kovacs J M, Lu X X, Flores-Verdugo F, Zhang C, Flores de Santiago F and Jiao X 2013 Applications of ALOS PALSAR for monitoring biophysical parameters of a degraded black mangrove (Avicennia germinans) forest *ISPRS J. Photogramm. Remote Sens.* **82** 102–11
[80] Lucas R *et al* 2010 An Evaluation of the ALOS PALSAR L-Band Backscatter—above ground biomass relationship Queensland, Australia: impacts of surface moisture condition and vegetation structure *IEEE J Sel Top Appl Earth Obs Remote Sens.* **3** 576–93
[81] Vreugdenhil M, Wagner W, Bauer-Marschallinger B, Pfeil I, Teubner I, Rüdiger C and Strauss P 2018 Sensitivity of sentinel-1 backscatter to vegetation dynamics: an austrian case study *Remote Sens.* **10** 1396
[82] Hall J, Muscarella R, Quebbeman A, Arellano G, Thompson J, Zimmerman J K and Uriarte M 2020 Hurricane-induced rainfall is a stronger predictor of tropical forest damage in Puerto Rico than maximum wind speeds *Sci Rep.* **10** 4318
[83] Mabry C M, Hamburg S P, Lin T-C, Horng F-W, King H-B and Hsia Y-J 1998 Typhoon disturbance and stand-level damage patterns at a subtropical forest in Taiwan *Biotropica.* **30** 238–50
[84] Morimoto J, Aiba M, Furukawa F, Mishima Y, Yoshimura N, Nayak S, Takemi T, Chihiro H, Matsui T and Nakamura F 2021 Risk assessment of forest disturbance by typhoons with heavy precipitation in northern Japan *For Ecol Manage.* **479** 118521
[85] Ostertag R, Silver W L and Lugo A E 2005 Factors affecting mortality and resistance to damage following hurricanes in a rehabilitated subtropical moist forest *Biotropica.* **37** 16–24
[86] Ostertag R, Scatena F N and Silver W L 2003 Forest floor decomposition following hurricane litter inputs in several Puerto Rican forests *Ecosystems.* **6** 261–73
[87] Cortés-Ramos J, Farfán L M and Herrera-Cervantes H 2020 Assessment of tropical cyclone damage on dry forests using multispectral remote sensing: The case of Baja California Sur, Mexico *J. Arid. Environ.* **178** 104171
[88] Lehmann E A, Caccetta P A, Zhou Z, McNeill S J, Wu X and Mitchell A L 2012 Joint processing of landsat and ALOS-PALSAR data for forest mapping and monitoring *IEEE Trans. Geosci. Remote Sens.* **50** 55–67
[89] Lu D and Weng Q 2007 A survey of image classification methods and techniques for improving classification performance *Int. J. Remote Sens.* **28** 823–70
[90] Reiche J *et al* 2016 Combining satellite data for better tropical forest monitoring *Nat Clim Chang.* **6** 120–2
[91] Cornforth W A, Fatoyinbo T E, Freemantle T P and Pettorelli N 2013 Advanced land Observing satellite phased array type L-band SAR (ALOS PALSAR) to Inform the conservation of mangroves: sundarbans as a case study *Remote Sens.* **5** 224–37
[92] McDowell N G *et al* 2015 Global satellite monitoring of climate-induced vegetation disturbances *Trends Plant Sci.* **20** 114–23
[93] Verhegghen A, Eva H, Ceccherini G, Achard F, Gond V, Gourlet-Fleury S and Cerutti P O 2016 The potential of sentinel satellites for burnt area mapping and monitoring in the congo basin forests *Remote Sens.* **8** 986